# Molecular weight effects on the stress-relaxation behavior of soft thermoplastic elastomer by means of temperature scanning stress relaxation (TSSR)

Simone Sbrescia, Tom Engels, Evelyne Van Ruymbeke, et al.

Citation: Journal of Rheology **66**, 1321 (2022); doi: 10.1122/8.0000444
View online: https://doi.org/10.1122/8.0000444
View Table of Contents: https://sor.scitation.org/toc/jor/66/6
Published by the The Society of Rheology

# Molecular weight effects on the stress-relaxation behavior of soft thermoplastic elastomer by means of temperature scanning stress relaxation (TSSR)

Simone Sbrescia,[1] Tom Engels,[2] Evelyne Van Ruymbeke,[1,a)] and Michelle Seitz[2]

[1]*Bio and Soft Matter Division (BSMA), Institute of Condensed Matter and Nanosciences (IMCN), Université catholique de Louvain, B-1348 Louvain-la-Neuve, Belgium*
[2]*DSM Materials Science Center, Urmonderbaan, 6167 RD Geleen, The Netherlands*

(Received 17 January 2022; final revision received 28 April 2022; published 1 November 2022)

**Abstract**

The mechanical properties of multiblock copolymer thermoplastic elastomers (TPEs) are governed by the interplay of different reversible dynamics [e.g., hard block (HB) association and chain entanglements]. Understanding how these physical processes influence the high-temperature deformation behavior is relevant as many TPEs lose toughness with increasing temperature. Increasing molecular weight (Mw) improves their temperature resistance that is attributed to an increase in network connectivity. Indeed, longer chains are characterized by more HBs per chain and by a longer lifetime of the entanglements in the amorphous phase. Both the associating HB and disentanglement dynamics are temperature and rate dependent. To further understand the interconnected role of Mw, temperature and rate dependencies on the mechanical properties, we perform Temperature Scanning Stress Relaxation (TSSR) tests. The method consists of measuring the stress relaxation of the materials as the temperature monotonically increases, allowing us to probe the stress response as the HBs progressively disassociate due to the increase in temperature. The results show that increasing Mw improves the high-temperature relaxation behavior, allowing the material to retain more stress than its low Mw counterpart as the temperature increases. This distinction does not show itself when performing standard small strain dynamic mechanical thermal analyses. Depending on the deformation experienced before the TSSR is performed, different relaxation behaviors are observed illustrating the importance of the current microstructure in determining the mechanical properties. The TSSR approach is well-suited to benchmark the high-temperature stress-bearing properties of network-based polymers whose morphology and, hence, properties are strongly deformation dependent. © *2022 The Society of Rheology.* https://doi.org/10.1122/8.0000444

## I. INTRODUCTION

The mechanical properties of multiblock copolymer thermoplastic elastomers (TPEs) are governed by the interplay of reversible hard block (HB) associations and chain entanglements. The resulting network topology is responsible for rubber-like elastic properties, coupled with melt processability and recyclability. TPEs are widely used in a variety of applications ranging from cables to shoe soles and have been extensively investigated in literature [1–4]. While TPEs generally show excellent fatigue and toughness at room temperature, the reversibility of these dynamics is also responsible for a decrease in toughness at high temperatures [5–7]. Understanding how the microstructure evolves and rearranges with deformation is critical as the recent work highlights that the ability of TPEs to resist crack propagation is strongly connected with structural reorganization occurring in local deformation zones [8,9].

Previously, we investigated the temperature- and deformation-dependent microstructure of TPEs and the impact of the morphology evolution with deformation on mechanical properties [7]. At low temperature and low deformations, the mechanical properties are mainly governed by the volume fraction of crystals [10], with little influence of Mw. With increasing deformation, the microstructure evolves via crystals breaking and orientation [1–4] into a microstructure where the small crystalline domains act as physical crosslinks and the entanglements are trapped between them (Fig. 1). At this stage, increasing Mw strongly increases the network elasticity and connectivity, resulting in stronger strain-hardening and higher strains at break [5,7] and lower rate-dependency of stress response [7]. Another way to reduce the size of the crystals is by increasing temperature. In such a case, melting of the crystals is observed, leading to the formation of smaller and weaker crystalline domains acting as physical crosslinks (Fig. 1).

In the present work, we propose that the relaxation behavior of a TPE to which high deformation is applied can also be explained by HB pull-out and chain-end disentanglement processes as observed in tensile tests. The latter processes have been described in our mechanistic model developed to explain the effects of Mw on the large-strain mechanical properties [7]. Briefly, the overall stress level at high deformations increases with the level of elastically active stress-bearing units (SBUs), i.e., with the number of crystallized HBs and entanglements. The number of SBUs decreases with increasing deformation or temperature as the HBs are pulled-out or thermally disassociate from the crystals and the amorphous phase disentangles. We assume that the disentanglement occurs only within the dangling-ends because

Note: This paper is part of the special issue on Double Dynamics Polymeric Networks

a)Author to whom correspondence should be addressed; electronic mail: evelyne.vanruymbeke@uclouvain.be

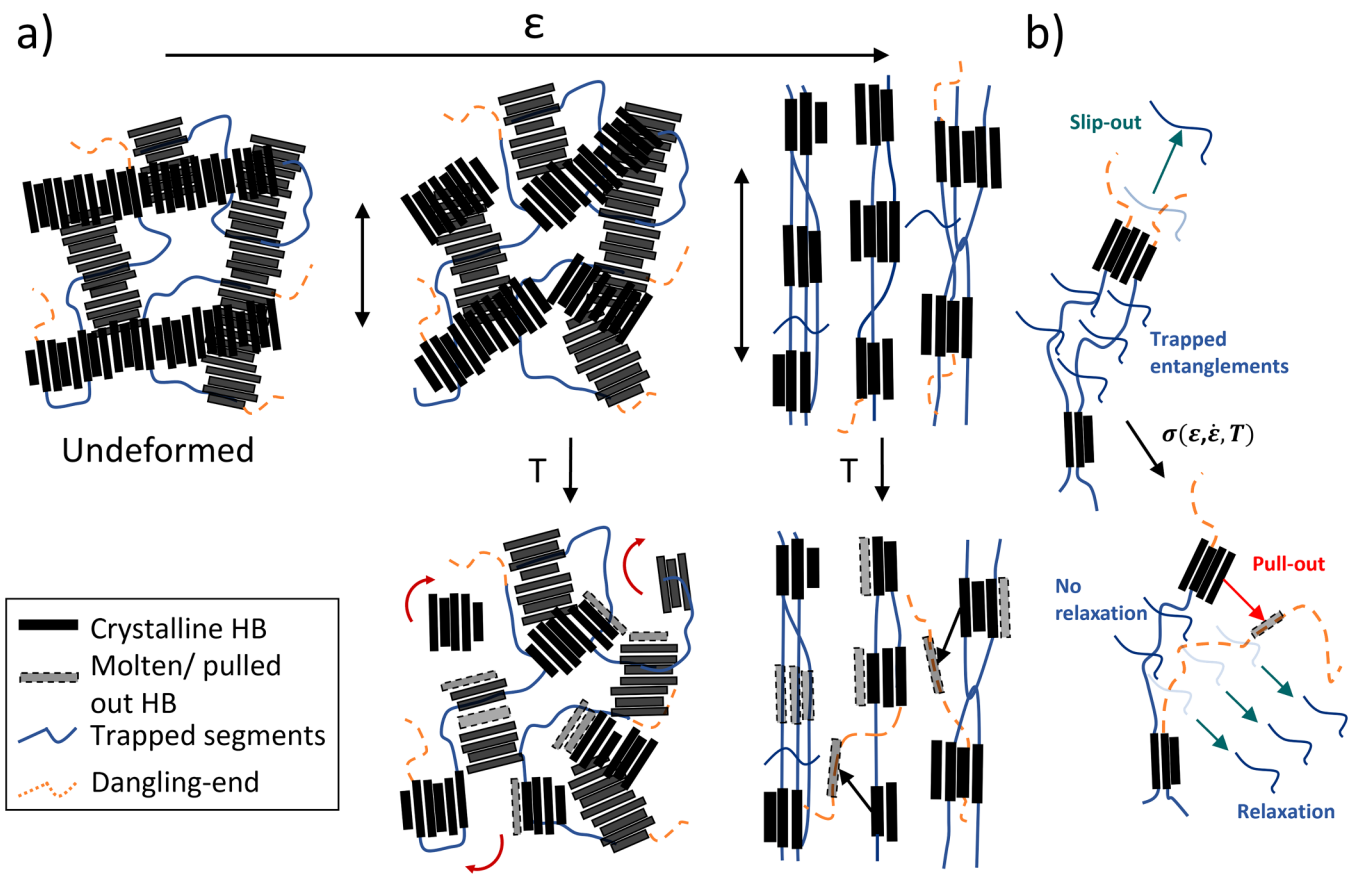


**FIG. 1.** (a) Schematic representation of the evolution of the microstructure with deformation (ε) and of the possible different relaxation processes occurring during the temperature (T) ramp. At small deformations, the stress is dominated by the interlocking network of crystals. With increasing T, the structure frees up with the melting of the crystals and reaches a lower-stress configuration. At large deformations, the stress response comes from the stretching of amorphous segments between entanglements and associated HBs. The relaxation originates from the cumulative temperature- and stress-induced pull-out of the HBs and chain-end disentanglement. (b) Schematic readapted from Ref. 7 representing the disentanglement, and consequent relaxation, occurring only in the dangling segments. As pull-out events occur, segments of chain are no longer trapped between two crystallized HBs and can now escape the entanglements and relax.

otherwise the entanglements are trapped between two crystallized HBs. The higher and less time-dependent stress response of the high-Mw network stems from the ability to better retain stresses or, in other words, to keep the amount of SBUs high at elevated temperatures, larger deformations, and longer times. Low-Mw samples are characterized by fewer HBs per chain and by short dangling-ends that disentangle rapidly favoring stress relaxation. Conversely, high-Mw samples have fewer and longer dangling ends leading to longer relaxation times in addition to having more HBs per chain. This allows the high-Mw chains to bear more stress even after high temperatures or stresses have resulted in several HB disassociation events.

The goal of this work is to gather additional experimental evidence for our morphological interpretation of the role of Mw on stress response [7]. To do so, we probe the relaxation response of the stretched networks as the HBs progressively disassociate from the crystalline domains due to an increase in temperature. According to the proposed model, at high deformations, high-Mw networks should relax less than low-Mw ones as the temperature increases.

The choice of probing the relaxation with temperature rather than with time, as it is conventionally done, is based on previous results that show that the temperature effect on the mechanical properties is significantly stronger than the time effect [5,7]. More importantly, the progressive temperature increase simulates a corresponding decrease in the fraction of associated HBs, which allows us to verify our mechanistic model by monitoring the stress response of samples with two different Mws. Additionally, studying the high-temperatures relaxation properties with conventional stress-relaxation methods can be challenging for this kind of materials. The long-term exposure at elevated temperatures can cause the crystalline domains to anneal during the measurement, significantly changing the structure under study. Hence, we base our study on the Temperature Scanning Stress Relaxation (TSSR) test [11–19], a recently developed testing protocol that allows us to rapidly screen the relaxation properties of polymer networks over a wide temperature range. The test consists of applying a constant deformation and measuring the corresponding decrease in stress during two consecutive steps:

(1) A first isothermal step at the temperature $T_0$; and
(2) A second nonisothermal step during which the temperature is monotonically increased at constant heating rate from $T_0$ to $T_f$.

The first step is analogous to a conventional stress relaxation test. The second one allows us to probe the relaxation response as the HBs progressively disassociate [20]. The

TSSR method as developed by Venneman and coworkers aims at obtaining a relaxation spectrum covering a broad relaxation time base. Traditionally, this is done by constructing a relaxation master curve by combining isothermal relaxation measurements over a wide range of temperatures using the time-temperature-superposition principle. Using linear elasticity and a generalized Maxwell model as the basis of their analysis, Venneman and coworkers now proposed to use the relaxation response obtained under a constant temperature ramp as the basis to obtain a relaxation spectrum and, by doing so, considerably shorten the required experimental effort since the continuously increasing temperature probes increasingly longer relaxation times. The technique was developed to obtain additional information on the complex molecular structure and phase behavior of TPEs by evaluating the elastic properties of their networks as a function of temperature, which would otherwise require a considerable effort with traditional tests [11]. The method has already been employed to characterize the relaxation behavior of TPEs, reversible and crosslinked elastomers, and their blends [11–19]. Here, we investigate the effect of Mw on the relaxation behavior of TPEs at a wider range of deformations, posing particular attention on the current state of the deformed microstructure and on the molecular dynamics influencing this behavior. Indeed, at low deformation, the stress bearing structure is represented by the mechanically interlocking network of crystals [3,7]. The stress level mainly scales with the volume fraction of crystals [10], which progressively decreases with increasing temperature [20]. At higher deformations, the crystals are broken, and the stress response mainly comes from the stretched and entangled amorphous segments trapped between the associated HBs [5,7]. With increasing temperature, the HBs disassociate, the amorphous phase disentangles, and the material relaxes.

This article starts with a description of the materials' chemistry and composition and of methods employed. Next, we summarize the materials' linear and nonlinear properties, which are helpful to contextualize the results obtained from the TSSR measurements that are presented next. First, we discuss the effect of Mw on the high-temperature relaxation behavior and then the effects of the deformational state of the microstructure. Finally, we use the TSSR results to calculate the crosslink density of the deformed microstructures and compare them with previous theoretical estimations.

## II. MATERIALS AND METHODS

The material is a poly(ether-ester) block copolymer based on polybutylene terephthalate (PBT) as HB and poly(tetramethylene oxide) (PTMO) as soft block (SB) obtained via transesterification followed by polycondensation of dimethyl terephthalate (DMT), 1,4-butanediol (BDO), and PTMO diol. The chemical structure is shown in Fig. 2. The catalyst used is tetrabutyl titanate (TBT), and the polyether is protected against oxidation during polymerization by 1,3,5-trimethyl-2,4,6-tris(3,5-di-*tert*-butyl-4-hydroxybenzyl) benzene [21]. The polycondensation reaction is carried out at 250 °C under vacuum, with a polymerization time of 200 min. The sequence length distribution from this type of polymerization follows the most probable form. After polymerization, the polymer is extruded as a strand and pelletized. The polymer granules are consequently dried at 100 °C for 2 h and at 140 °C for 5 h. The samples are made of 40% in weight of HB and characterized by SB with an average length of 2 kg/mol. Two different total chain Mws are tested, 29 and 50 kg/mol, which we refer to as 60_PTMO2k_29 and 60_PTMO2k_50, respectively, and are identical to the materials studied in Ref. 7. 200 $\mu$m thick films are prepared following the same procedure described previously [7]. Relevant materials' structural parameters are shown in Table I.

Rectangular samples, $2 \times 10\,\text{mm}^2$, are cut from the films. To avoid slippage of the sample from the grips, an additional material taken from the same films is placed between the sample and the surface area of the grips. The TSSR procedure employed in previous studies [11–17] is mimicked on a RSA-3 TA Instrument (USA). The samples are preloaded to 0.05 N (ca. 0.12 MPa) before the test starts. The sample is first taken to 50 °C at a rate of 2 °C/min before stretching to avoid strain-induced crystallization of SBs [7,21–24]. Next, the sample is stretched to $\varepsilon \sim 20\%$ or $\sim 200\%$, followed by 2 h of isothermal stress relaxation. Additional tests with a target strain of $\sim 500\%$ are performed by prestretching the samples in a Zwick Roell (Germany) 1474 Universal tensile testing machine prior to the TSSR measurement. The results and the details on the sample preparation are shown Fig. S1 [40]. Finally, the heating ramp starts at a rate of 2 °C/min up to 175 °C. The drop of the stress ratio is recorded both during isothermal relaxation and the temperature scan. A schematic of the protocol is shown in Sec. III.

## III. RESULTS AND DISCUSSIONS

### A. Linear and nonlinear mechanical properties: Effect of Mw and deformation-induced microstructure

Figure 3 shows the results from mechanical tests performed in linear and nonlinear regimes obtained in our

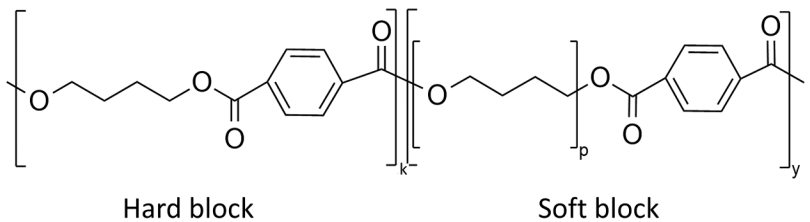


**FIG. 2.** Chemical structure of the PBT-PTMO block copolymer. The HB is a sequence of k PBT (DMT + BDO) monomers.

**TABLE I.** Structural parameters.

| Samples | SB wt (%) | $M_{n,SB}$ [I] (kg/mol) | E′ (50 °C) [II] (MPa) | E′ (100 °C) [II] (MPa) | <*N*> [III] (–) | $T_m$ peak [IV] (°C) | Mw [V] (kg/mol) |
|---|---|---|---|---|---|---|---|
| 60_PTMO2k_29 | 60 | 2 | 40.9 | 25.4 | 6.5 | 200 | 29 |
| 60_PTMO2k_50 | 60 | 2 | 38.3 | 23.0 | 11.2 | 205 | 50 |

I. Number average molecular weight of the SB diol.
II. Storage modulus measured at 50 or 100 °C from DMTA measurements reported in Ref. 7.
III. Average number of associated HBs per chain at T = RT estimated following the method described in Ref. 20.
IV. PBT melting peak maximum extracted from DSC second heating at 10 °C/min [7].
V. Number average molecular weight of the total chains.

previous work with Dynamic Mechanical Thermal Analysis (DMTA) and tensile tests, respectively [7]. The results indicate clear differences in the mechanical properties when increasing Mw only in the nonlinear regime, highlighting the importance of the deformation-induced microstructure and its connectivity in determining the mechanical properties. On the contrary, in the linear regime, the storage modulus (Fig. 3(a)), the loss modulus [Fig. 3(b)], and loss angle [tan(δ)] [Fig. 3(c)] are hardly influenced by the chain length; the small difference in the absolute modulus level is due to differences in the crystalline volume fraction [10]. The storage modulus gradually decreases with increasing temperature as a result of progressive melting of PBT crystals, starting from the least perfect ones [20,25]. At temperatures above 150 °C, the storage modulus of the low-Mw sample drops more sharply than the high-Mw one. The reason for this is not yet clearly understood. One possibility is that the volume fraction of crystals decreases with increasing temperature [20] until the crystals stop being mechanically interlocked and the contribution of the entanglements to the modulus becomes more significant. At this stage, a higher modulus is expected from the high-Mw, being characterized by fewer dangling-ends and more trapped entanglements. However, this is of secondary importance as we observe differences in the relaxation behavior and in the nonlinear mechanics in general, already at T << 150 °C. The similarities in the loss angle between the two samples indicate no differences in the relaxation behavior in the linear regime.

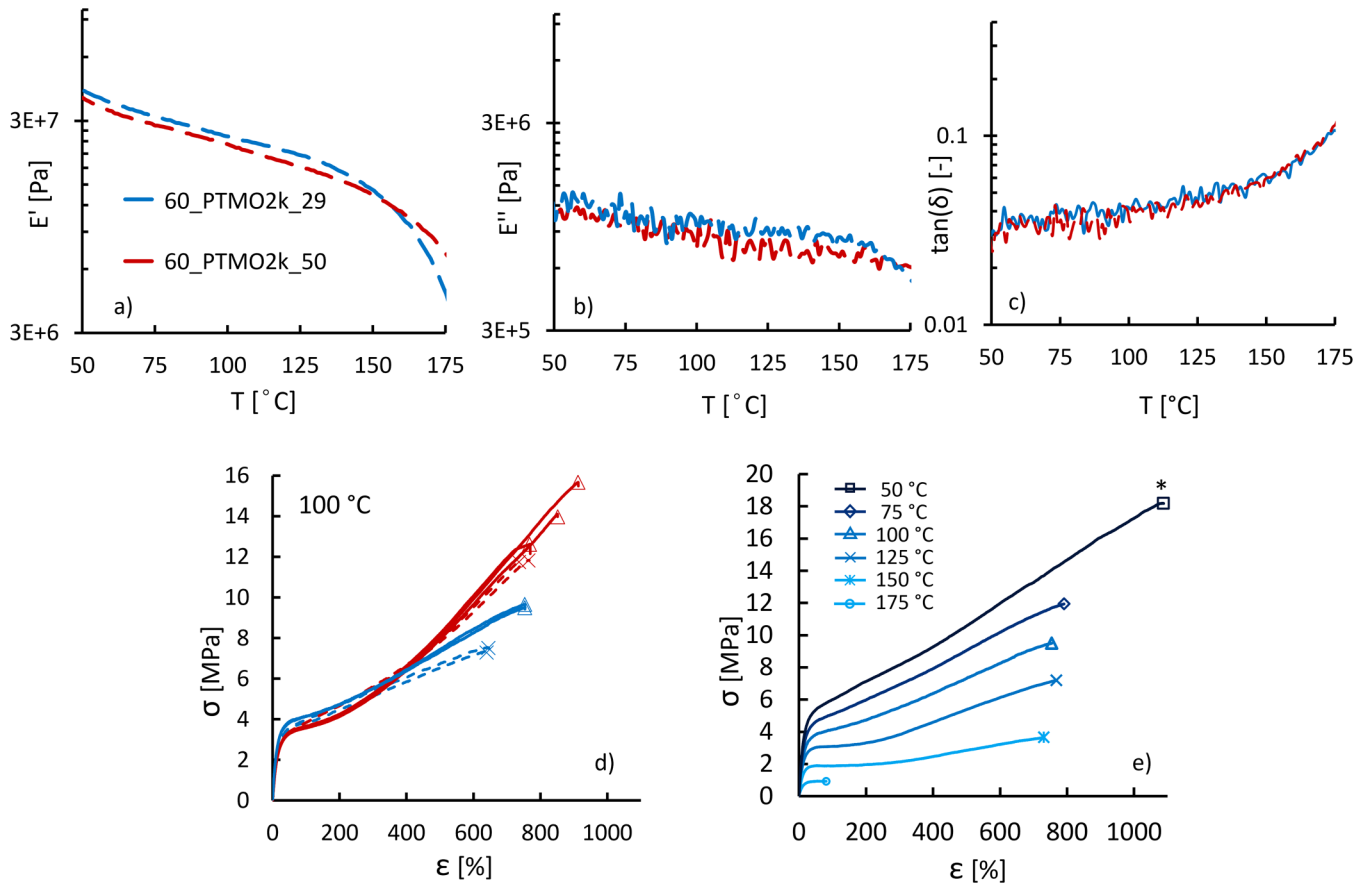


**FIG. 3.** Storage (a) and loss (b) modulus and tan(δ) (c) from DMTA measurements between 50 and 175 °C performed at 5 °C/min, with a constant frequency of 1 Hz and 1% of strain amplitude. (d) Engineering stress-strain curves performed at 100 °C and at 500 mm/min (continuous line) and 5 mm/min (dashed lined). Original curves shown in [7]. (e) Engineering stress-strain curves performed at different temperatures and at 500 mm/min on the sample 60_PTMO2k_29. The star for the 50 °C curve denotes that the sample did not fail before the crosshead displacement limit was reached.

During continuous loading [Fig. 3(d)], little difference is seen with varying Mw up to $\varepsilon \approx 300\%$ after which increasing Mw leads to increased strain hardening and failure strain. Analogous results were also observed in previous studies [3,5]. However, cyclic tests showed increased strain recovery with increasing Mw for samples stretched already at $\varepsilon \approx 100\%$ [7]. Hence, we expect differences in network connectivity and, thus, in the stress relaxation response, with varying Mw for strains at least higher than 100%. Additionally, Fig. 3(d) shows that the strain-hardening response of the low-Mw samples is much more rate-dependent; with increasing deformation rate, the strain-hardening response increases. As described in the Introduction, this can be explained by considering better connectivity of the high-Mw samples, which results into longer dangling-ends during deformation, with longer relaxation times, which translates into a longer lifetime of the SBUs in the network [7]. The large influence of temperature on the strain and stress at break is illustrated in Fig. 3(e).

Starting from these results, we would like to examine the results obtained with TSSR measurements in the nonlinear regime on samples with two different Mws. As noted above, at higher strains, the microstructure is different from the one in the linear regime, and the stress response (and its relaxation) is governed by different mechanisms. In particular, it must be considered that while in the linear range the HB dissociation events are induced by temperature, at higher deformations both temperature and stress cause pull-out of the HBs from the crystals. Hence, we would like to discuss the effects that the temperature- and stress-induced pull-out and disentanglement events have on the relaxation properties, compare them with the results obtained in the linear regime, and assess consistency with our mechanistic model.

### B. Stress relaxation: Network elasticity increases with Mw

The TSSR experimental procedure is schematically depicted in Fig. 4 along with the results obtained for isothermal stress relaxation at 50 °C (step III) shown in the absolute scale (a) and in terms of the ratio (c) relative to the maximum stress reached during stretching ($\sigma_0$). At this temperature and within the 2 h test time, the relaxation behavior does not vary significantly with Mw. Figures 4(b) and 4(d) show the relaxation occurring during the temperature ramp (step IV) in the absolute and relative scale, respectively. For the latter, the stress reached after the 2 h isothermal step is used as a reference value ($\sigma_1$). In contrast to isothermal relaxation at 50 °C, we observe a difference in relaxation behavior during the temperature ramp with Mw for both applied strain levels. Analogous observations can be made for the samples stretched at 500% (Fig. S1) [40].

The lack of influence of Mw during isothermal relaxation at 50 °C suggests no significant differences in terms of loss of connectivity or breaking of the crystals between the two samples at the testing temperature and at the imposed levels of stretching. To further test the validity of this theory, we performed an isothermal stress relaxation test at 100 °C and

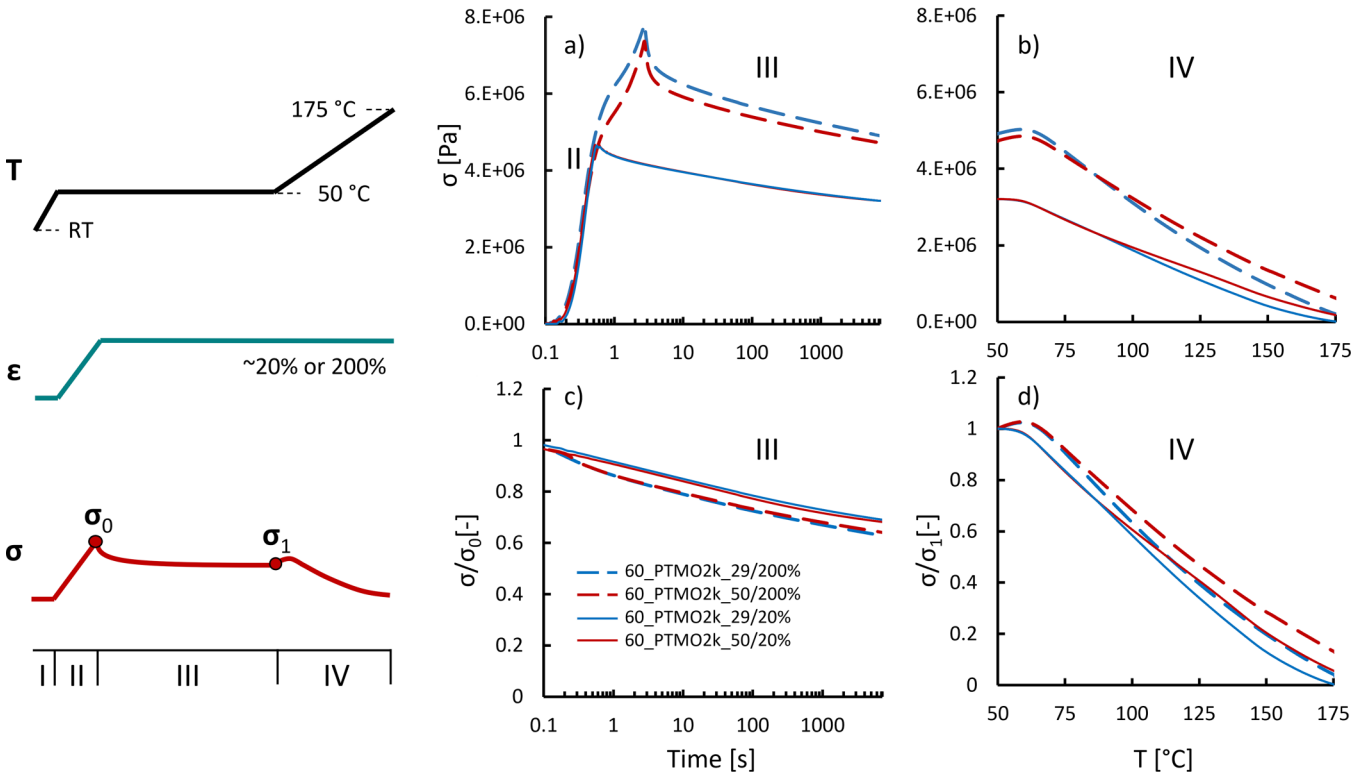


**FIG. 4.** (Left) Schematic of the TSSR procedure, ε and T are imposed and the stress σ is measured. (Right) Stress relaxation during the isothermal step (a) and the temperature ramp (b). Stress ratio drop during isothermal (c) and temperature ramp (d). $\sigma_0$ is the maximum stress reached during stretching, while $\sigma_1$ is the stress reached at the end of the isothermal step. In (a), the initial time corresponds to the start of the deformation to show the loading curve as well. In (c), the initial time corresponds to the starting point of the relaxation, i.e., right after the target strain is reached. Figure S1 [40] includes the results obtained for the samples stretched to ~500%. Values for $\sigma_0$ and $\sigma_1$ can be found Table S1 [40].

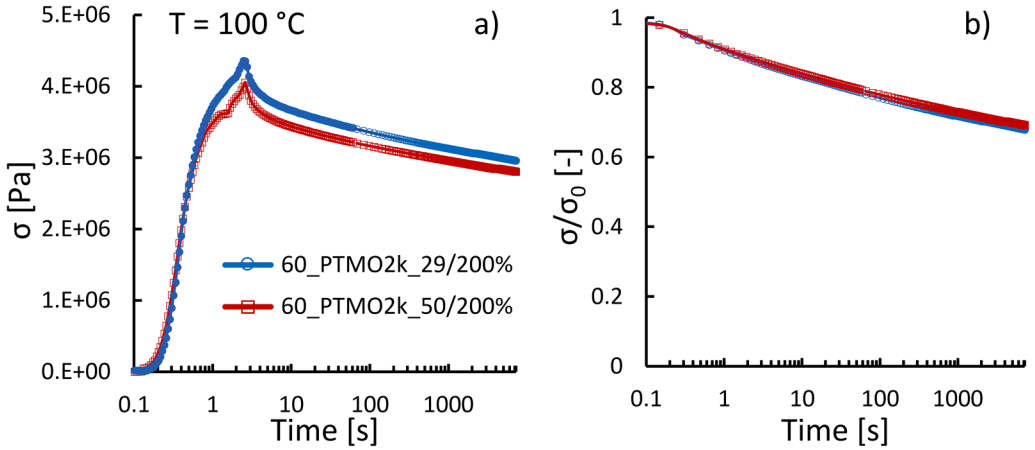


**FIG. 5.** Isothermal stress relaxation tests performed at 100 °C for samples stretched at ~200% of strain in the absolute (a) and relative (b) scale. $\sigma_0$ corresponds to the maximum stress reached during loading (see Fig. 4) and corresponds to 4.4 and 4.1 MPa for the low- and high-Mw samples, respectively.

at 200% of strain. The results, as shown in Fig. 5, show again no substantial differences in the relaxation behavior when varying Mw in isothermal conditions. However, we do not exclude that at sufficiently high temperatures, stress-induced HB pull-out occurs in the isothermal condition, which would result in differences in the stress relaxation response between the low and high Mw samples. Indeed, in isothermal conditions, it is not easy to find a temperature or time window to probe the differences in network connectivity and in the consequent stress response with varying Mws.

With increasing temperature, partial melting of PBT crystals occurs, and connectivity decreases. As a result, some chain segments, previously trapped between two crystallized HBs, become dangling ends that are free to relax. With increasing Mw, the probability of a chain segment becoming a dangling end decreases and their relaxation times increase [7]. Consistent with the expectation from the mechanistic model, the high-Mw sample relaxes less during the temperature ramp, confirming that the more elastic high-Mw network retains stresses better than the low-Mw one as HB disassociation events progressively occur with increasing temperature. Additionally, while there are no significant differences in the linear regime at $T < 150$ °C, we observe differences in the relaxation behavior with varying Mw already at $T \sim 75$ °C. This can be explained by considering the different natures of stress response between linear and nonlinear regimes, stemming from their different microstructures. In the former, the stress mostly scales with the volume fraction of crystals [10] and is little influenced by Mw [5,7]. Only at high T (>150 °C), does considerable crystal melting occur resulting in HBs disassociation and allowing the chains to relax. In the nonlinear regime, the HB disassociation events are induced cumulatively by temperature and stress. Therefore, the effect of Mw already appears on the stress relaxation at lower temperatures, as the stress response depends on network connectivity, itself strongly influenced by Mw [7].

It must be noted that in the investigated temperature range, the high-Mw sample has a slightly lower storage modulus than the low-Mw sample, which reflects slight differences in the crystalline volume fraction. Additionally, the two samples have an almost identical loss modulus and same tan(δ) [Table I and Figs. 3(a)–3(c)], which may lead to incorrect expectation that they would relax similarly. In actuality, the high-Mw sample relaxes much less during the TSSR test. Again, the differences between the results obtained in linear and nonlinear regimes originate from the differences in the microstructures and, hence, properties between the less and more highly stretched samples. Thus, in contrast to crosslinked rubbers, where the elasticity is fully governed by the crosslinking density, the high-strain elasticity in TPEs depends critically on network connectivity and network topology. The latter is strongly temperature-dependent and deformation-dependent. Next, we discuss the effects of deformation on the relaxation properties and connect them with the microstructural changes.

### C. Stress relaxation: Influence of deformation and microstructure on the relaxation behavior

Figures 4(c) and 4(d) show the results relative to two different target deformations. During the isothermal step (III), the less-stretched samples show slightly less relaxation than the highly stretched ones. This is consistent with previous results on low- and high-density polyethylene where it has been shown that the degree of relaxation increases with the drawing ratio [26–29]. Indeed, the authors show that higher deformations lead to more oriented molecules, to more strain hardening, and to a stronger driving force to relax to lower conformational stresses. Furthermore, their higher local stresses could additionally favor chain pull-out from the crystals [5], especially when the temperature is increased. This leads to differences in the sample microstructure, which governs the overall chain mobility. Indeed, with increasing deformation, the crystals progressively break up into smaller ones [1–4] and the overall chain mobility increases, favoring stress relaxation.

During the temperature ramp [Fig. 4(d)], the stress ratio of less-stretched samples is lower at each temperature than that of higher stretched samples. Increasing the temperature significantly affects the relaxation behavior by increasing the molecular mobility and progressively melting the crystals, starting from the least perfect ones [20,21,30]. As

schematically depicted in Fig. 1, in the case of the less deformed microstructure, it is possible that decreasing the volume fraction of crystals by increasing the temperature frees the polymer chains that can rearrange further to decrease the stress. In this case, the relaxation behavior is mainly driven by chain mobility, which is hampered by crystals and facilitated by the presence of dangling-ends. At high deformations, the microstructure is instead less restricted by the volume fraction of the (broken) crystals, the latter being not interlocked anymore [3,7] but is kept taut by small crystal domains acting as physical crosslinks and by the entanglements trapped between them [31]. This can be observed in Fig. 4(d), where the stress ratio of the highly stretched material initially increases with temperature due to entropic network effects: below 60 °C, the small crystal domains are stable and act as chemical crosslinks. However, at higher temperature, the temperature-induced pull out of the HBs becomes significant and the stress relaxation overcomes the entropic effect. As explained before, one chain can relax via pull-out from the crystal domains followed by the disentanglement, hence, only when an end-chain HB gets pulled out from a crystal domain followed up by the disentanglement of the freed-up dangling segment. The likelihood of this event strongly decreases with increasing Mw [7]. These results highlight the importance of accounting for the current state of the microstructure when studying the time and temperature dependency of the stress response of these materials [32,33]. Different strain-induced microstructures lead to different relaxation behaviors.

To summarize, the TSSR results show that the stress relaxation with increasing temperature is significantly affected by Mw and deformation, in agreement with the mechanistic picture previously proposed [7]. We investigated the stress relaxation at both 20% and 200% (and at 500%, Fig. S1)[40] of prestretch as a function of Mw, showing that the elastic behaviors of TPE networks stretched to different extents are different and possibly driven by distinct physical processes. Interestingly, we observe clear differences in the high-temperature relaxation behavior with varying Mw already at 20% of the prestretch, whereas during tensile continuous loading [Fig. 3(d)], significant differences in the transient stress-strain response are only observed above ~300% of strain. These results demonstrate that TSSR, similarly to cyclic tests [7,20,34], is sensitive to network connectivity of TPEs at much lower strains than standard tensile tests.

### D. Crosslink density

The TSSR method can also be used to estimate the crosslink density of the stretched network [11–19]. After 2 h of isothermal relaxation, ideally, most of the material's viscous contributions have relaxed. With increasing temperature, the stress ratio initially increases due to entropic network effects [Figs. 4(b)–4(d)]. Afterward, relaxation overcompensates the entropic effect, and the stress ratio drops again. For an ideal entropy-elastic network, the engineering stress is proportional to the temperature [35] as

$$\sigma = \nu RT\left(\lambda - \frac{1}{\lambda^2}\right), \tag{1}$$

where $\nu$ is the crosslink density, $R$ is the ideal gas constant, and $\lambda$ is the draw ratio ($\lambda = \varepsilon/100 + 1$). In order to estimate $\nu$, we applied Eq. (1) in the temperature range from 50 to 55 °C. The correct calculation includes a correction for $\nu$ that accounts for the fact that at the beginning of the temperature ramp the materials are not fully relaxed. Indeed, the slow, ongoing stress relaxation partially compensates for the entropy effect. Details on how the correction is performed are reported in [11] and are summarized Table S2 [40]. The estimated ν from TSSR leads to values around ~700 mol/m$^3$, which are comparable to the values theoretically predicted [see Fig. 6(a)] by considering as crosslinks the associated HBs and the stress-bearing entanglements, following the model developed in our previous work [7], which leads to the following equation for ν:

$$\nu = [1 - f_{dang}(f)]\left(\frac{\rho}{M_e}\right) + (1 - f)\langle N\rangle\left(\frac{\rho}{M}\right), \tag{2}$$

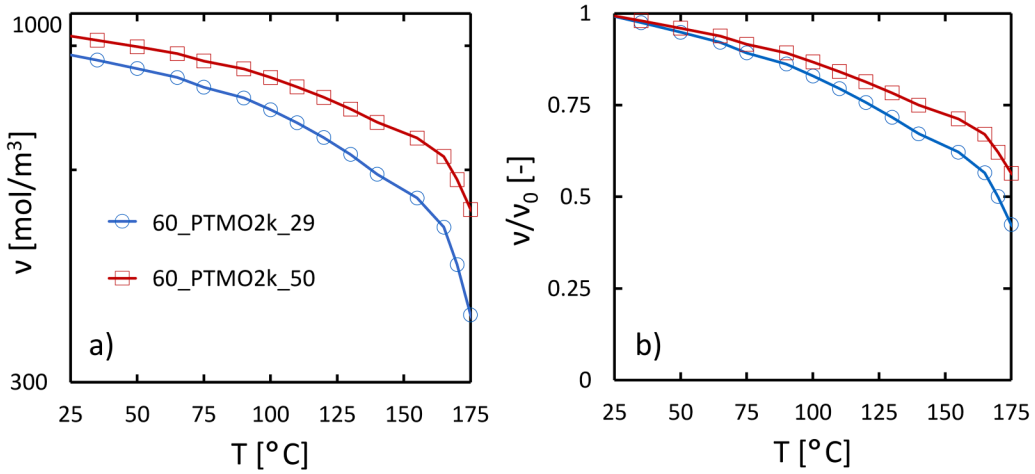


**FIG. 6.** (a) Crosslink density ν estimated as the density of stress bearing segments between associated HBs and entanglements versus temperature following Eq. (2). (b) Relative decrease in the crosslink density versus temperature with respect to the value at T = RT ($\nu_0$).

where $f_{dang}$ is the fraction of dangling-ends, $f$ is the fraction of disassociated HBs, $\rho$ is the polymer density (1.1 g/cm$^3$), $M_e$ is the molecular weight between entanglements (~1.4 kg/mol [36]), $\langle N \rangle$ is the average number of associated HBs, and $M$ is the molecular weight of the chains, here assumed to be monodisperse. Details on how all the parameters in Eq. (2) are estimated can be found in our previous work [7]. In the latter, $f$ is an independent parameter. Here, we approximate $f$ with the fraction of HBs that melt at a given temperature, which can be estimated if the HB length distribution is known [20]. Briefly, the HB length polydispersity leads to a broad range of melting temperatures, which can be described using Flory's theory of crystallization of block copolymers [26] At each temperature, a minimum HB length exists [$k$*(T)], expressed in terms of PBT monomer repeat units, below which crystals cannot form. In the case of random distribution of HB lengths, i.e., with a PBT monomer sequence propagation probability equal to the mole fraction of PBT monomers ($x_{PBT}$), the average number of HBs per chain that are longer than $k$*(T) and, hence, can crystallize and contribute as physical crosslinks can be estimated as [37]

$$\langle N \rangle = n^*(1 - x_{PBT})^*(x_{PBT})^{k^*(T)}, \tag{3}$$

where $n$ is the average degree of polymerization of the total chain. It must be pointed out that Flory's theory assumes unrestricted mobility of the sequences of same chains when crystallization occurs and excludes any kinetics of crystallization. Thus, the values of $\langle N \rangle$ estimated from this model will be higher than those observed experimentally. Estimated values of $\langle N \rangle$ at T = RT are reported in Table I.

Equation (3) gives us a reasonable estimation of how $\langle N \rangle$ decreases with increasing temperature, which allows us to estimate $f$ as

$$f = 1 - \frac{\langle N \rangle(\mathrm{T})}{\langle N \rangle(\mathrm{T} = \mathrm{RT})}. \tag{4}$$

It must be noted that this approximation does not account for an increase in $f$ that occurs during stretching due to HB pull-out.

Combining Eqs.(2)–(4) allows us to estimate how the crosslink density decreases with increasing temperature. The results, shown in Fig. 6, show a progressive decrease in the crosslink density with increasing temperature, which is consistent with the results from TSSR in Fig. 4. ν ranges from ~900 mol/m$^3$ at RT to ~800 mol/m$^3$ at 100 °C, down to ~500 and ~400 mol/m$^3$ at 175 °C for high and low Mw samples, respectively, and is consistent with estimations obtained with the TSSR method.

One more way to estimate the network crosslink density is to consider the slopes of the stress-strain curves measured at high strains [38], analogously to what it has been done in Eq. (1). For example, using the Gaussian model, as shown in Fig. 7, allows us to express the network modulus (G) as

$$\mathrm{G} = A\nu\mathrm{RT}, \tag{5}$$

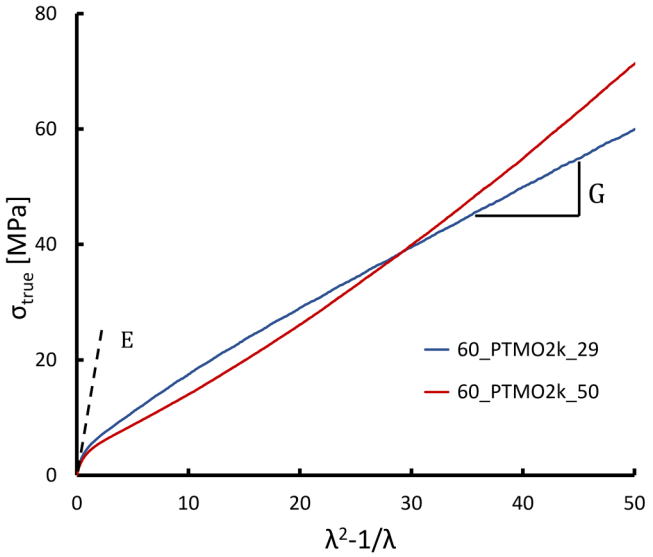


**FIG. 7.** True stress versus $\lambda^2$–$1/\lambda$ plots corresponding to the stress-strain curves at 100 °C and 500 mm/min as shown in Fig. 3(d) up to a $\varepsilon \approx 600\%$. The calculation of G is performed in $200\% < \varepsilon < 500\%$ and leads to $\mathrm{G} = 1.08 \pm 0.01$ MPa and $\mathrm{G} = 1.35 \pm 0.01$ MPa for low- and high-Mw samples, respectively.

where R is the ideal gas constant and $A$ is a prefactor that depends on network model assumption. In the case of affine network model, $A = 1$. According to the phantom network model and considering the entanglements as tetrafunctional crosslinks, $A = 1/2$. Due to the complex viscoelastic behavior and the strain-dependent morphology, the real material's behavior is far more complex than Gaussian, but the affine and phantom network models provide reasonable lower and upper bounds, respectively, for the determination of ν [39].

Following this approach by calculating G from the experimental stress-strain curves collected at 100 °C, as shown in Fig. 3(d), leads to ν ranging from ~350 mol/m$^3$ ($A = 1$) to ~700 mol/m$^3$ ($A = 1/2$) for the low-Mw sample and from ~450 mol/m$^3$ ($A = 1$) to ~900 mol/m$^3$ ($A = 1/2$) for the high-Mw sample. The results are of the same magnitude of model predictions, and the estimations with TSSR fall in the same range. However, it should be considered that the strain hardening behavior of these materials during loading is affected by viscous dissipation (molecular friction and crystal breaking and orientation) and that, as said above, the real deformation is far from phantom and affine network model assumptions.

The values of ν are of the same magnitude when calculated from TSSR, stress-strain curves, or from theory, and, as expected, all the methods show an increase in ν with increasing Mw. However, we note that these differences are small and should not be overinterpreted.

The overall agreement between the theoretical and measured data supports the idea that once stretched, the morphology evolves toward one close to an entangled crosslinked rubber, with crystalline HB domains acting as physical crosslinks. This picture is further supported by the fact that the entropic contribution coming from the temperature increases, i.e., the initial increase in the stress ratio at the starting of the temperature ramp, is visible only for highly stretched

samples [see Figs. 4(b)–4(d) or zoomed-in version Fig. S2] [40]. For the samples deformed at modest strains, the crystal network is expected to dominate the stress response rather than the entropic response of the amorphous strands, and hence, we would not expect an increase in the stress ratio with increasing temperature at low strain levels.

## IV. SUMMARY AND CONCLUSIONS

In this work, we adopted the TSSR approach to gather relaxation data on TPEs to investigate the influence of Mw on their high-strain response. From uniaxial tensile and cyclic tests performed in our previous work, we observed increasing strain-hardening and elastic recovery with increasing Mw over a wide temperature range. We proposed these effects to originate from better network connectivity and longer lifetime of the chain-end entanglements with increasing Mw resulting in more stress retention at each stage of deformation. The results in this work are consistent with this picture and support our mechanistic model by showing that increasing Mw leads to increased stress retention as the temperature progressively increases. Thus, increasing Mw is an effective strategy to improve the high-temperature relaxation behavior of TPEs, with little influence on the linear and low-strain mechanical properties, albeit at the cost of increased viscosity and potential processing challenges. We also demonstrate that the TSSR approach has value for quickly screening the temperature-dependent relaxation properties and estimating the crosslinking density of TPEs or any network-based polymer whose morphology is strongly temperature- and deformation-dependent.

Additionally, this study highlights the importance of accounting for deformation-induced structural changes in determining the mechanical properties and, in particular, the relaxation behavior. Acknowledging and understanding this is critical for tackling problems where the material is subjected to inhomogeneous stress and strain fields resulting in inhomogeneous microstructure and properties, for example, applications with complex designs or during fracture. The importance of the deformation-induced structural changes in fracture mechanics is highlighted by recent studies [8,9] showing that the ability of TPEs to resist crackpropagation is strongly linked to the structural reorganization occurring in local deformation zones.

## ACKNOWLEDGMENTS

This work was financially supported by funding from the H2020 Program (MARIE SKŁODOWSKA-CURIE ACTIONS) of the European Commission's Innovative Training Networks (No. H2020-MSCA-ITN-2017) under DoDyNet REA Grant Agreement No. 0.765811. EVR id Research Associate of the FRS-FNRS. The authors thankfully acknowledge Anouk van Graven for the support with the DMTA and TSSR tests.

## AUTHOR DECLARATIONS

### Conflict of Interest

The authors have no conflict to disclose.

## DATA AVAILABILITY

The data that support the findings of this study are available from the corresponding author upon request.

## REFERENCES

[1] Fakirov, S., *Handbook of Condensation Thermoplastic Elastomers* (Wiley-VCH, Weinheim, 2005).

[2] Konyukhova, E. V., V. M. Neverov, Y. K. Godovsky, S. N. Chvalun, and M. Soliman, "Deformation of polyether-polyester thermoelastoplastics: Mechanothermal and structural characterisation," Macromol. Mater. Eng. **287**, 250–265 (2002).

[3] Gaymans, R. J., "Segmented copolymers with monodisperse crystallizable hard segments: Novel semi-crystalline materials," Prog. Polym. Sci. **36**, 713–748 (2011).

[4] Zhu, P., X. Dong, and D. Wang, "Strain-induced crystallization of segmented copolymers: Deviation from the classic deformation mechanism," Macromolecules **50**, 3911–3921 (2017).

[5] Aime, S., N. D. Eisenmenger, and T. A. P. Engels, "A model for failure in thermoplastic elastomers based on Eyring kinetics and network connectivity," J. Rheol. **61**, 1329–1342 (2017).

[6] Auriemma, F., C. De Rosa, M. Scoti, R. Di Girolamo, A. Malafronte, M. Christian D'Alterio, L. Boggioni, S. Losio, A. Caterina Boccia, and I. Tritto, "Structure and mechanical properties of ethylene/1-octene multiblock copolymers from chain shuttling technology," Macromolecules **52**, 2669–2680 (2019).

[7] Sbrescia, S., J. Ju, T. Engels, E. Van Ruymbeke, and M. Seitz, "Morphological origins of temperature and rate dependent mechanical properties of model soft thermoplastic elastomers," J. Polym. Sci. **59**, 477–493 (2021).

[8] Scetta, G., E. Euchler, J. Ju, N. Selles, P. Heuillet, M. Ciccotti, and C. Creton, "Self-organization at the crack tip of fatigue-resistant thermoplastic polyurethane elastomers," Macromolecules **54**, 8726–8737 (2021).

[9] Scetta, G., N. Selles, P. Heuillet, M. Ciccotti, and C. Creton, "Cyclic fatigue failure of TPU using a crack propagation approach," Polym. Test. **97**, 107140 (2021).

[10] Nébouy, M., A. Louhichi, and G. P. Baeza, "Volume fraction and width of ribbon-like crystallites control the rubbery modulus of segmented block copolymers," J. Polym. Eng. **40**, 715–726 (2020).

[11] Venneman, N., *Characterization of Thermoplastic Elastomers by Means of Temperature Scanning Stress Relaxation Measurements. Thermoplastic Elastomers* (InTech, Rijeka, 2012), pp. 347–370.

[12] Skulrat, P., C. Nakason, and N. Vennemann, "Thermoplastic elastomers-based natural rubber and thermoplastic polyurethane blends," Iran. Polym. J. **21**, 65–79 (2012).

[13] Anagha, M. G., T. Chatterjee, and K. Naskar, "Assessing thermomechanical properties of a reactive maleic anhydride grafted styrene-ethylene-butylene-styrene/thermoplastic polyurethane blend with temperature scanning stress relaxation method," J. Appl. Polym. Sci. **137**, 48727 (2020).

[14] Vennemann, N., K. Bökamp, and D. Bröker, "Crosslink density of peroxide cured TPV," Macromol. Symp. **245-246**, 641–650 (2006).

[15] Barbe, A., K. Bökamp, C. Kummerlöwe, H. Sollmann, N. Vennemann, and S. Vinzelberg, "Investigation of modified SEBS-based thermoplastic elastomers by temperature scanning stress relaxation measurements," Polym. Eng. Sci. **45**, 1498–1507 (2005).

[16] Chatterjee, T., S. Hait, A. B. Bhattacharya, A. Das, S. Wiessner, and K. Naskar, "Zinc salts induced ionomeric thermoplastic elastomers based on XNBR and PA12," Polym. Plast. Technol. Mater. **59**, 141–153 (2020).

[17] Pichaiyut, S., C. Nakason, C. Kummerlöwe, and N. Vennemann, "Thermoplastic elastomer based on epoxidized natural rubber/thermoplastic polyurethane blends: Influence of blending technique," Polym. Plast. Technol. Mater. **23**, 1011–1019 (2012).

[18] Chatterjee, T., N. Vennemann, and K. Naskar, "Temperature scanning stress relaxation measurements: A unique perspective for evaluation of the thermomechanical behavior of shape memory polymer blends," J. Appl. Polym. Sci. **135**, 45680 (2018).

[19] Das, A., A. Sallat, F. Böhme, E. Sarlin, J. Vuorinen, N. Vennemann, G. Heinrich, and K. W. Stöckelhuber, "Temperature scanning stress relaxation of an autonomous self-healing elastomer containing non-covalent reversible network junctions," Polymers **10**, 94 (2018).

[20] Sbrescia, S., T. Engels, E. Van Ruymbeke, and M. Seitz, "Effect of block length on the network connectivity and temperature resistance of model, soft thermoplastic elastomers," J. Rheol. **66**, 177–185 (2022).

[21] Gabriëlse, W., M. Soliman, and K. Dijkstra, "Microstructure and phase behavior of block copoly (ether ester) thermoplastic elastomers," Macromolecules **34**, 1685–1693 (2001).

[22] Schmidt, A., W. S. Veeman, V. M. Litvinov, and W. Gabriëlse, "NMR investigations of in-situ stretched block copolymers of poly (butylene terephthalate) and poly (tetramethylene oxide)," Macromolecules **31**, 1652–1660 (1998).

[23] Litvinov, V. M., M. Bertmer, L. Gasper, D. E. Demco, and B. Blümich, "Phase composition of block copoly (ether ester) thermoplastic elastomers studied by solid-state NMR techniques," Macromolecules **36**, 7598–7606 (2003).

[24] Zhu, P., C. Zhou, Y. Wang, B. Sauer, W. Hu, X. Dong, and D. Wang, "Reversible–Irreversible Transition of Strain-Induced Crystallization in Segmented Copolymers: The Critical Strain and Chain Conformation," ACS Applied Polymer Materials **3**, 3576–3585 (2021).

[25] Flory, P. J., "Theory of crystallization in copolymers," Trans. Faraday Soc. **51**, 848–857 (1955).

[26] Djoković, V., D. KosTOSKI, M. D. Dramićanin, and E. Suljovrujić, "Stress relaxation in high density polyethylene: Effects of orientation and gamma radiation," Polym. J. **31**, 1194–1199 (1999).

[27] Boiko, Y. M., W. Brostow, A. Y. Goldman, and A. C. Ramamurthy, "Tensile, stress relaxation and dynamic mechanical behavior of polyethylene crystallized from highly deformed melts," Polymer **36**, 1383–1392 (1995).

[28] Boiko, J. M., V. V. Kovriga, and A. J. Goldman, "Stress relaxation in highly oriented polyethylene," Plaste Kautsch. **40**, 192 (1993).

[29] Djoković, V., Z. Kačarević-Popović, D. Dudić, and D. Kostoski, "Effect of gamma irradiation on the stress-relaxation of drawn LLDPE," Polym. Degrad. Stab. **61**, 73–77 (1998).

[30] De Almeida, A., M. Nébouy, and G. P. Baeza, "Bimodal crystallization kinetics of PBT/PTHF segmented block copolymers: Impact of the chain rigidity," Macromolecules **52**, 1227–1240 (2019).

[31] Riise, B. L., G. H. Fredrickson, R. G. Larson, and D. S. Pearson, "Rheology and shear-induced alignment of lamellar diblock and triblock copolymers," Macromolecules **28**, 7653–7659 (1995).

[32] Hsiue, G. H., D. J. Chen, and Y. K. Liew, "Stress relaxation and the domain structure of thermoplastic elastomer," J. Appl. Polym. Sci. **35**, 995–1002 (1988).

[33] Long, D., and P. Sotta, "Stress relaxation of large amplitudes and long timescales in soft thermoplastic and filled elastomers," Rheol. Acta **46**, 1029–1044 (2007).

[34] Buckley, C. P., D. S. A. De Focatiis, and C. Prisacariu, "Unravelling the mysteries of cyclic deformation in thermoplastic elastomers," in *Constitutive Models for Rubber VII* (CRC Press, 2011), pp. 3–10.

[35] Mark, J. E., "Rubber elasticity," J. Chem. Educ. **58**, 898 (1981).

[36] Das, C., D. J. Read, M. A. Kelmanson, and T. C. McLeish, "Dynamic scaling in entangled mean-field gelation polymers," Phys. Rev. E **74**, 011404 (2006).

[37] Frensdorff, H. K., "Block-frequency distribution of copolymers," Macromolecules **4**, 369–375 (1971).

[38] Men, Y., J. Rieger, and G. Strobl, "Role of the entangled amorphous network in tensile deformation of semicrystalline polymers," Phys. Rev. Lett. **91**, 095502 (2003).

[39] Mark, J. E., *Physical Properties of Polymers Handbook* (Springer, New York, 2007).

[40] See supplementary material at https://www.scitation.org/doi/suppl/10.1122/8.0000444 for additional details on TSSR measurement, for the results on the sample stretched at ∼500%, and for details on the corrections for the calculation of the crosslink density.